Surface Nanometer-Scale Patterning in Realizing Large-Scale Ordered Arrays of Metallic Nanoshells with Well-Defined Structures and Controllable Properties

By *Shikuan Yang, Weiping Cai,* Lingce Kong,* and *Yong Lei**

Surface patterns of nanoshell arrays play an important role in diverse applications including surface-enhanced Raman scattering (SERS) sensors, lithium-ion batteries, solar cells, and optical devices. This paper describes an innovative surface nanopatterning technique for realizing large-scale ordered arrays of metallic spherical nanoshells with well-defined structures. Ag nanoshell arrays are prepared using polystyrene sphere templates by an electrophoretic process in Ag colloidal solutions. The fabricated Ag nanoshell arrays have a high controllability of the structural parameters, including the diameter, the surface roughness, and the intershell spacing, giving rise to the tunable properties of nanoshell arrays. As an example, tunable SERS and localized surface plasmon resonance of the nanoshell arrays are demonstrated by controlling the structural parameters. The surface nanopatterning technique shown in this paper is a general fabrication process in achieving not only metallic nanoshell arrays, but also nanoshell arrays of semiconductors and metallic oxides.

1. Introduction

The unique properties of functional nanoshell structures (especially hollow shells) are of great importance in diverse application areas, such as the substrates for surface-enhanced Raman scattering (SERS) sensors,[1,2] the electrodes in lithium-ion batteries[3–5] or solar cells,[6] and the fundamental structures in optical devices (e.g., a wave guide).[7] In most of these applications, it is highly desirable to prepare large-scale arrays of nanoshells on a substrate (mainly a semiconductor wafer) for the device integration. In particular, in order to tailor the properties of devices based on the nanoshell arrays, it is technologically required to fabricate regularly arrayed patterns of nanoshells with well-defined structures. Recently, the searching for an efficient and low-cost nanopatterning technique to fabricate nanoshell arrays has involved developments of technologies based on nanoscale kirkendall effect,[8] self assembly,[9–11] galvanic replacement,[12–14] surface coating of oxide particles, [15–17] and so on. However, fabrication of large-scale surface patterns of nanshells with well-defined structures and controllable properties is almost impossible using these processes. The development of an efficient surface nanopatterning technique with practical routes to synthesize large-scale ordered arrays of nanoshells with high structural and property controllability presents an important issue in the field of surface nanopatterning.

In this article, we present a novel surface nanopatterning technique for fabricating large-scale ($\sim$1 cm^2) ordered arrays of metallic nanoshells with well-defined structures. The fabrication of Ag nanoshell arrays is based on an electrophoretic process in Ag colloidal solutions using monolayer polystyrene (PS) sphere templates as the electrophoretic electrodes. The structural parameters of the Ag nanoshell arrays are well-controlled, including the diameter and the surface roughness of the nanoshells, and the spacing between the neighboring nanoshells. Properties of the nanoshell arrays including SERS and localized surface plasmon resonance (LSPR) can be controlled based on structural control of the nanoshells. The Ag nanoshell array consisting of 60 nm sized nanoparticles and with 20 nm intershell spacing shows highest SERS enhancement, which could be used as the SERS substrate with high sensitivity.

[*] Prof. W. P. Cai, Dr. S. K. Yang
Key Laboratory of Materials Physics, Anhui Key Laboratory of Nanomaterials and Nanotechnology, Institute of Solid State Physics, Chinese Academy of Sciences
Hefei 230031 (China)
E-mail: wpcai@issp.ac.cn
Prof. Y. Lei, Dr. S. K. Yang
Institute of Materials Physics and Center for Nanotechnology
University of Muenster
Muenster 48149 (Germany)
E-mail: yong.lei@uni-muenster.de
Prof. Y. Lei
Institute of Nanochemistry and Nanobiology
Shanghai University
Shanghai 201800 (China)
L. C. Kong
The Third Department
Institute of Chemical Defence
Beijing 102205 (China)

DOI: 10.1002/adfm.201000467

2. Results and Discussion

2.1. Fabrication Strategy of Ag Nanoshell Arrays

Ag nanoshell arrays were synthesized using an electrophoretic deposition process (Fig. 1). Monolayer PS sphere template on a

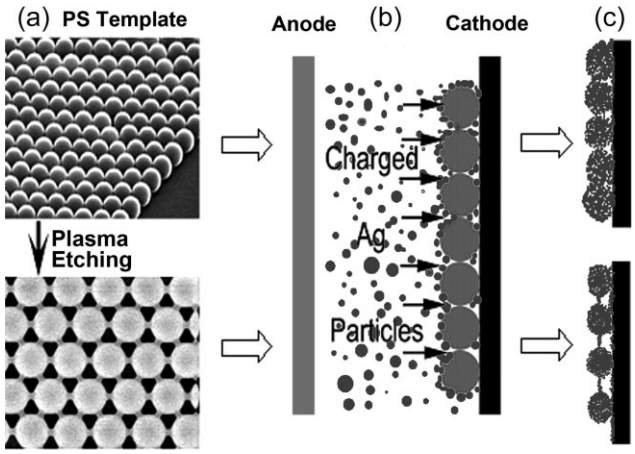

Figure 1. Fabrication strategy of Ag nanoshell arrays using an electrophoretic process in Ag colloidal solutions induced by laser ablation. a) As-prepared close-packed PS sphere template and non-close-packed PS sphere template after plasma etching. b) Electrophoretic process in the Ag colloidal solution. c) Ag nanoparticles attached on the PS spheres, forming close-packed and non-close-packed Ag nanoshell arrays.

substrate [Si wafer or indium tin oxide (ITO) glass] were used as the cathodes of the electrophoretic process (Fig. 1a). Before the electrophoretic process, a thin Ag layer (about 3 nm in thickness) was deposited on the PS sphere template. The electrophoretic deposition was carried out in the Ag colloidal solution, which contains nearly spherical Ag particles with about 10 nm in mean size and was prepared by laser ablation of an Ag flake in water (the details can be found in the Experimental section). Due to the charged surfaces of the Ag nanoparticles in the colloidal solution, Ag nanoparticles were electrophoretically deposited on the electrode (i.e., PS sphere template), forming Ag nanoshells on PS spheres (Fig. 1b,c).

Using a plasma etching process on as-prepared close-packed PS sphere arrays (Fig. 2a), non-close-packed PS sphere arrays can be synthesized with crosslinked bars between the neighboring PS spheres (Fig. 2b). The spacing between the non-close-packed PS spheres (i.e., the length of the crosslinked bars) depends on the etching time, and the bars can be removed by a subsequent thermal treatment process (Fig. 2b, inset). Both the close-packed and non-close-packed PS sphere arrays can be used as the templates for the electrophoretic growth of Ag nanoshells (Fig. 1c). The PS spheres inside the Ag nanoshells can be removed by a chemical etching process using toluene, giving rise to ordered arrays of hollow spherical nanoshells.

A typical Ag nanoshell array on a Si wafer is shown in Figure 3a, in which highly roughened surfaces of nanoshells are demonstrated. The nanoshells are composed of many tiny Ag nanoparticles, and crevices with a very high density (more than 10^3 per shell[18]) are formed between the nanoparticles (Fig. 3a, inset). XRD measurement (Fig. 3b) shows the face-centered-cubic (fcc) crystalline structures of Ag. TEM observation reveals the uniform structures of the nanoshells (Fig. 3c) while the selected area electron diffraction (SAED) pattern further confirms the fcc structures of the Ag nanoshells (Fig. 3c, inset).

Here, it should be mentioned that the pre-evaporated Ag thin film on the surfaces of PS spheres is of great importance for the

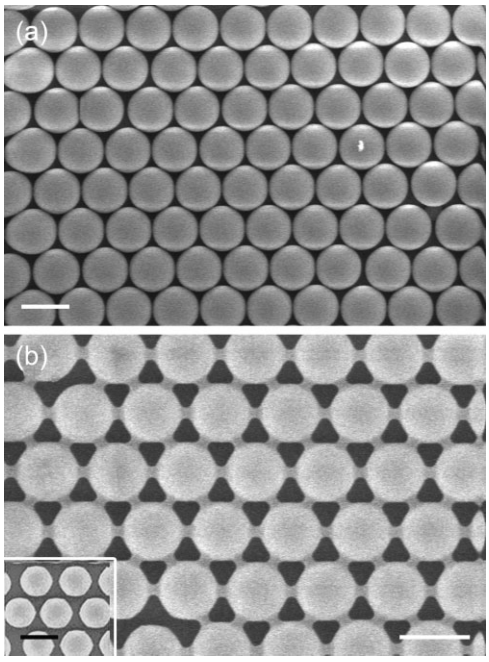

Figure 2. SEM images of the monolayer PS sphere arrays: close-packed PS spheres (a) and non-close-packed PS spheres (b). The Inset in (b) shows the removal of the crosslinked bars between the PS spheres using a thermal treatment process at 110 °C for 10 min. Scale bars: 750 nm.

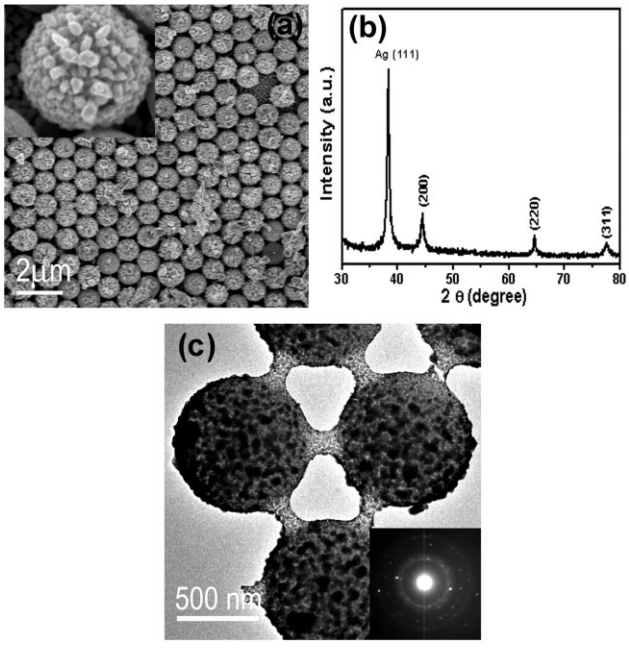

Figure 3. a) Morphology (SEM, top-view) of Ag nanoshell arrays prepared on 1 μm-sized PS spheres under 100 μA cm^{-2} electrophoretic current density, the inset is an enlarged view of a nanoshell. b) XRD result shows the face-centered-cubic crystalline structure of Ag. c) TEM results of Ag nanoshells, the inset is the SAED pattern that confirms the fcc structures of the Ag nanoshells.

growth of Ag nanoshells. Without this thin Ag film, Ag particles will deposit in the clearance of PS spheres and there is no nanoshell formed on PS spheres. Further, it is found that both the mobility of Ag nanoparticles in the solution and the subsequent crystal growth through the oriented connections between nanoparticles act together, leading to size's evolution of the nanoparticles in the electrophoretic process, as previously reported.[19] The electrophoresis induced crystal growth of Ag nanoparticles in the nanoshells is clearly shown in a long-time-deposition sample shown in Figure S1.

2.2. High Structural Controllability

The diameter of Ag nanoshells mainly depends on the diameter of PS spheres.[20] Since the diameter of PS spheres can be controlled from about 200 nm to 4.5 μm, the diameter of Ag nanoshells can be adjusted in a similar size range. Ag nanoshells with diameters of about 1000 and 750 nm are shown in Figure 3 and Figure 4, respectively.

Besides the diameters, the spacing between the neighboring nanoshells can also be adjusted. Figure 4 shows non-close-packed Ag nanoshell arrays with different intershell spacings. As mentioned above, the spacing between the PS spheres (i.e., the length of the crosslinked bars) depends on the etching time of the plasma etching process. By choosing different etching time in preparing the PS sphere templates (corresponding to the different inter-sphere spacings), the spacing between the neighboring Ag nanoshells can be controlled. As shown in Figure 4, the spacing of the nanoshells increases with the plasma etching time, resulting in intershell spacing of about 20 nm with 1 min etching time (Fig. 4b), 35 nm with 2 min (Fig. 4c), 65 nm with 3 min (Fig. 4d), 90 nm with 6 min (Fig. 4e), and 110 nm with 10 min (Fig. 4f). Correspondingly, the diameter of the Ag nanoshells decreases with the etching time, from about 750 nm in the beginning, to 730, 715, 685, 660, and 640 nm, respectively. Therefore, the plasma etching time can be used to modify both the intershell spacing and the diameter of the Ag nanoshells.

Interestingly, it is found that the size of the Ag nanoparticles in nanoshells can be adjusted by controlling the electrophoretic current density. Figure 5a–c shows non-close-packed nanoshells prepared under current densities of 10, 50, and 100 μA cm^{-2}, respectively, which indicates that the size of nanoparticles increases with the current density. The size distribution as a function of the electrophoretic current density is shown in Figure 5d. The mean size of nanoparticles is about 25, 40, and 60 nm when the current density is 10, 50, and 100 μA cm^{-2}, respectively. Since the surface roughness of Ag nanoshells is mainly determined by the mean size of the Ag nanoparticles in the nanoshell, the surface roughness of nanoshells can be controlled based on the size adjustment of nanoparticles.

Based on the above, the structural parameters of the Ag nanoshell arrays can be adjusted triply: First, the diameter of the Ag nanoshells can be tuned from about 200 nm to 4.5 μm based on the diameter adjustment of PS spheres. Moreover, the nanoshell diameter can be modified by the plasma etching time of PS templates. Second, the surface roughness of the Ag nanoshells is controllable by selecting appropriate electrophoretic current densities. Third, the spacing between the neighboring nanoshells can be controlled by choosing different PS spheres with different inter-sphere spacings (a range between 20 to 110 nm of the intershell spacing is shown in Fig. 4).

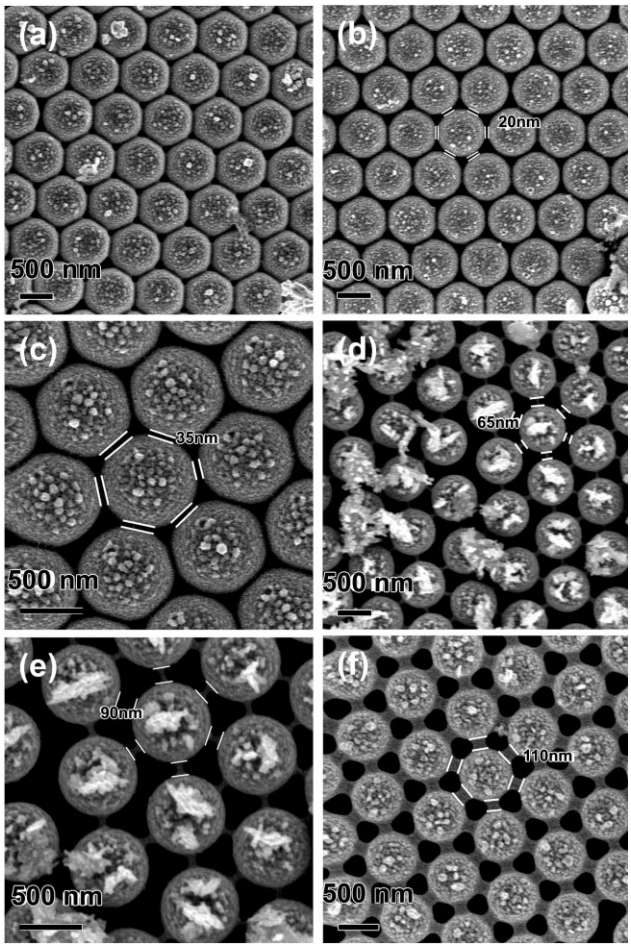

Figure 4. SEM images (top view) of a set of six samples showing the spacing controlling of Ag nanoshells based on the adjustment of the plasma etching time of PS sphere templates (diameter of PS spheres is about 750 nm before etching). The electrophoretic current and time for fabricating the Ag nanoshells are 50 μA cm^{-2} and 9 h, respectively. The average intershell spacing of the Ag nanoshells can be controlled by the plasma etching time: a) close-packed (no etching), b) 20 nm (1 min), c) 35 nm (2 min), d) 65 nm (3 min), e) 90 nm (6 min), and f) 110 nm (10 min). The intershell spacing is marked in each image. Correspondingly, the diameter of the Ag nanoshells decreases with the etching time, from about 750 nm (a), to 730 nm (b), 715 nm (c), 685 nm (d), 660 nm (e), and 640 nm (f).

2.3. Tunable SERS and LSPR properties

The high structural controllability of Ag nanoshell arrays can be used to tune their properties. In this work, the dependence of the LSPR and SERS properties of Ag nanoshells arrays on their structures were investigated systematically. It is well known that

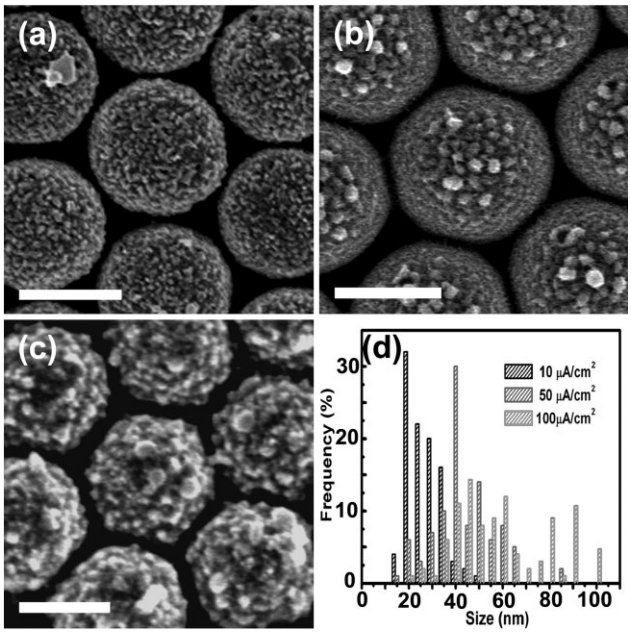

Figure 5. SEM images of Ag nanoshell arrays synthesized under different electrophoretic deposition current densities: a) 10 μA cm^{-2}, b) 50 μA cm^{-2}, c) 100 μA cm^{-2}. Scale bars: 500 nm. d) The size distributions (acquired by counting more than 200 nanoparticles) of the Ag nanoparticles in nanoshells. The mean size of nanoparticles is about 25, 40, and 60 nm when the current density is 10, 50, and 100 μA cm^{-2}, respectively, the deviations are 25 ± 10 nm, 40 ± 25 nm, and 60 ± 30 nm.

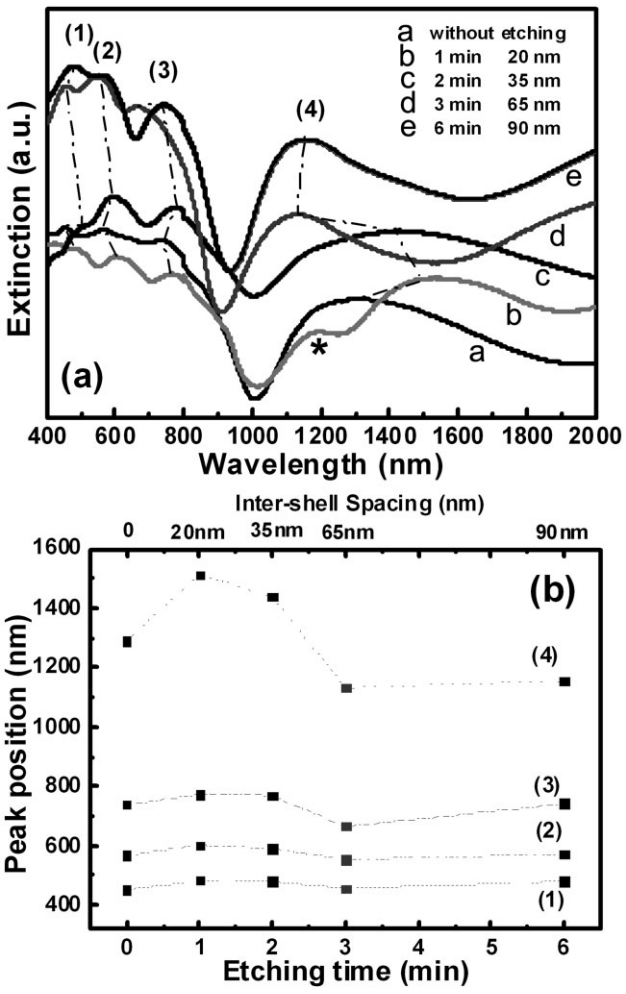

Figure 6. a) UV-vis-NIR extinction spectra of the five Ag nanoshell samples with different intershell spacing (shown in Fig. 4a–e). b) Shifting of the peak positions of the main four peaks marked in panel (a) with the plasma etching time and the intershell spacing.

the LSPR and SERS performance of noble metal (Au and Ag) nanostructured arrays depends on both the morphology of the building blocks and the geometric parameters of the whole assembly. In our case, three factors can be used to adjust the LSPR and SERS properties: i) the intershell spacing and ii) the diameter of nanoshells, and iii) the mean size of the nanoparticles in nanoshells.

UV-vis-NIR absorption spectra of the nanoshell arrays prepared under the current density of 50 μA cm^{-2} (corresponding to the five samples in Fig. 4a–e) are shown in Figure 6a, which clearly illustrates that the intershell spacing has prominent influence on the LSPR properties. There are four LSPR peaks located from the visible to the near IR range. And these four peaks have the similar evolutions regarding the shifting of the peak position as a function of the intershell spacing (Fig. 6b). When the spacing is about 20 nm, the LSPR peaks red-shift compared with those of the close-packed nanoshell arrays. Moreover, an additional LSPR peak at 1190 nm appears (the asterisk mark in Fig. 6a). Further increasing of the intershell spacing to about 35 nm stops the red-shifting of the peak positions, and a blue-shifting starts, especially for the peaks (2) and (4). As the spacing increases to about 65 nm, the LSPR peaks have prominent blue-shifts to high energy levels. Further enlargement of the spacing to about 90 nm results in small red-shifts. Similar relations of the LSPR shifting with the intershell spacing are observed for the nanoshell arrays prepared under the current densities of 10 and 100 μA cm^{-2}.

The size of the Ag nanoparticles (controlled by the current density) can also be used to tune the LSPR of the Ag nanoshells. Figure 7a gives the absorption spectra of Ag nanoshell arrays, corresponding to the three samples in Figure 5 that were prepared under different electrophoretic current densities. As shown in Figure 7b, the LSPR peaks blue-shift with the increase of the mean size of nanoparticles (i.e., increase of the current density).

Figure 8a shows SERS spectra of Rhodamine 6G (R6G) molecules adsorbed on Ag nanoshells with different intershell spacings (corresponding to the five samples in Fig. 4a–e). It is clearly shown that the nanoshell array with about 20 nm spacing has strong Raman peaks (curve b) with intensities of more than 5 times of those of the close-packed one (curve a). The intensity of the Raman signal decreases with the increasing of the intershell spacing (from 20 to 35, 65, and 90 nm). Further investigation shows that the diameter of nanoshells also influences the SERS enhancement. Arrayed nanoshells with diameters of about 2 μm show much weaker SERS signal (curve α) than those of the nanoshells with diameters in the range of 660–750 nm (all the other lines except curve α in Fig. 8a).

Furthermore, Ag nanoshell arrays with different sizes of Ag nanoparticles have different SERS enhancement. As shown in

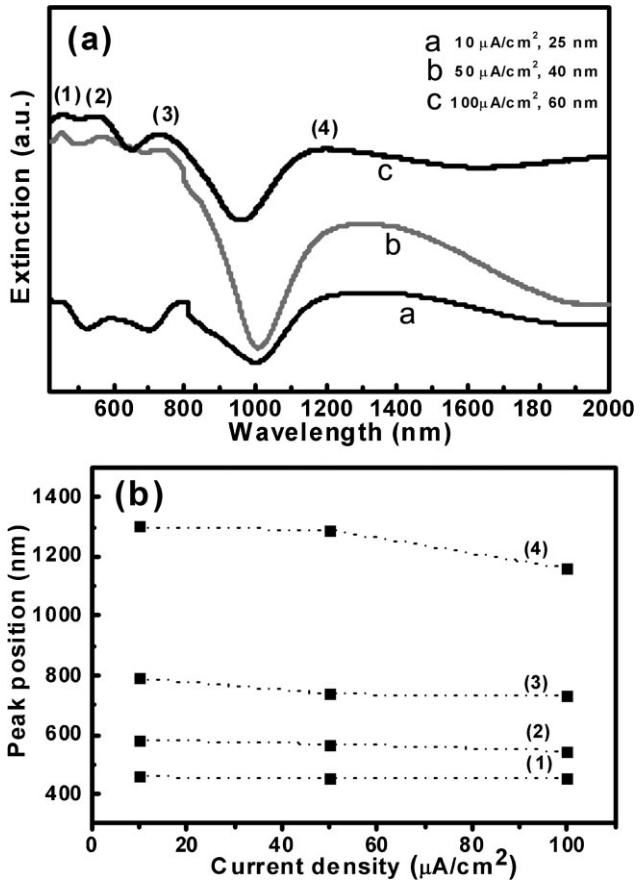

Figure 7. a) UV-vis-NIR extinction spectra of the three Ag nanoshell samples fabricated using different current densities (the three samples in Fig. 5 with different mean sizes of the nanoparticles in the nanoshells). b) Shifting of the peak positions of the main four peaks marked in panel (a) with the deposition current density.

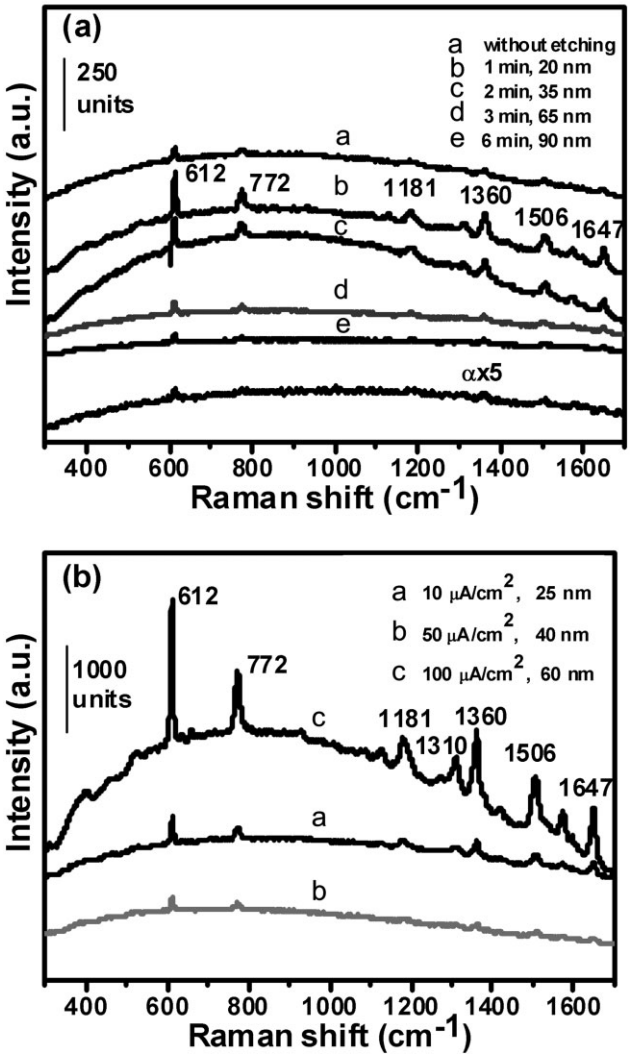

Figure 8. a) SERS spectra of Rhodamine 6G (R6G) molecules adsorbed on Ag nanoshells with different intershell spacing (the five samples in Fig. 4a–e). Curve α is the SERS curve (5 times enlarged) of Ag nanoshells with diameter of about 2 μm. b) SERS spectra of R6G molecules adsorbed on Ag nanoshells with different size of nanoparticles (the three samples in Fig. 5). All the SERS data are averaged by 5 scans over randomly chose areas and the standard deviation is less than 10%.

Figure 8b, the effect of the nanoparticle size on the SERS signal is more prominent than that of the intershell spacing. It is found that the SERS enhancement of nanoshells with 25 nm sized Ag nanoparticles is about 3 times higher than that of the nanoshells with 40 nm sized particles, while the nanoshells with 60 nm sized particles have the strongest SERS signal (about one magnitude higher than that of the nanoshells with 40 nm sized particles).

2.4. Structural Parameter Dependent Coupling Effects

As we know, nanoparticles that are much smaller than the wavelength of visible light have only dipole plasmon resonance.[21] When the size of particles increases, multipole plasmon modes start. The multipole plasmon modes appear at higher energy range than that of the dipole plasmon resonance in the extinction spectrum, which is known as phase retardation effect. Nanoshells have the similar size-dependent plasmon resonance performance to that of nanoparticles. There are some reports concerning the dipole plasmon properties of noble metal nanoshells with the size smaller than 100 nm, such as single shell and two neighboring shells.[22–27] Ag nanoshells with relatively large diameter (500–1000 nm) in this work support higher order multipole plasmon resonance. According to plasmon hybridization theory,[22] the interaction of the inner and outer surface of nanoshells results in the splitting of plasmon resonances into two new resonances. Therefore, higher order multipole modes are excited in the shell layers and participate in the plasmon hybridization, results in the LSPR features shown in Figure 6a. The dipole and quadrupole interaction gives rise to the appearance of peaks (3) and (4), while peaks (1) and (2) are caused by even higher order multipole interactions such as quadrupole and octupole. The plasmon coupling between arrayed nanoshells with larger shell spacing (e.g., 90 and 65 nm) is weak, which is similar to the LSPR

performance of single nanoshells. As the spacing decreases to 35 nm, the LSPR hybridization between the neighboring nanoshells is enhanced, resulting in the red-shifting of the plasmon peaks to the lower energy level. When the spacing reaches 20 nm, the plasmon hybridization is further enhanced, giving rise to further red-shifted LSPRs. And the strong coupling between the dipole plasmon modes results in the peak at about 1190 nm (the asterisk mark in Fig. 6a), leading to a complete separation of the dipole hybridization from the quadrupole hybridization. As to the close-packed nanoshells that are connected to each other, electrons flow across the adjacent nanoshells. The consequent blue-shifting counteracts the red-shifting of LSPR peaks caused by the plasmon coupling, resulting in the LSPR shifting to high energy level (curve a in Fig. 6). Moreover, the nanoshell thickness increases with the size of the Ag nanoparticles in the nanoshell. Thus the plasmon coupling between the inner and outer surface of nanoshells is weakened, leading to the LSPR blue-shifting shown in Figure 7.

Strong plasmon coupling will produce intense near-field electromagnetic fields (''hot spots'') between adjacent nanoshells,[28–30] thus generating periodically located hot spots (with large SERS enhancement) across the nanoshell arrays. Therefore, the strong plasmon coupling existing in the nanoshell arrays with 20 nm intershell spacing should give rise to a strong SERS enhancement. The SERS enhancement should be weakened when the spacing increases to 35, 65, and 90 nm, which agrees well with the experimental results (Fig. 8a). Concerning the arrayed Ag nanoshells with diameter of about 2 μm, a much lower density of hot spots in the nanoshell arrays than that of the nanoshells with 750 nm in diameter results in a much lower Raman signal intensity.

The surface roughness of nanoshells is more dominant for the SERS enhancement than the intershell spacing. As previously reported,[31,32] Ag nanoparticles with the size range within 60–100 nm show intense SERS enhancement. In our case, Ag nanoshells formed with 60 nm sized nanoparticles exhibit the best SERS enhancement due to three reasons. First, nanoparticles with about 60 nm in mean size have intense SERS enhancement. Second, the large number of crevices (nanogaps) between the nanoparticles further induce the SERS enhancement. Third, the nanoscale spacings between the neighboring nanoshells also magnify the SERS signal. It is found that arrayed Ag nanoshells consisting of 60 nm mean sized nanoparticles and with 20 nm intershell spacing have the strongest SERS enhancement, which could be used for the SERS substrates with high sensitivity. We estimated the SERS enhancement factors of this sample [using 4-aminothiopheno (4-ATP) as probe molecules for the Raman measurement, as shown in Fig. S2] by the equation:

$$EF = (I_{SERS}/N_{ads})/(I_{bulk}/N_{bulk}) \quad (1)$$

where EF is the enhancement factor; I_{SERS} and I_{bulk} are the Raman signal intensities at 1075 cm^{-1}, which is a representative vibration of 4-ATP molecules adsorbed on the nanoshell array and the bulk 4-ATP, respectively; N_{ads} and N_{bulk} are the numbers of 4-ATP molecules absorbed on the nanoshell arrays and the solid 4-ATP exposed to the laser spot, respectively. Based on this calculation, the enhancement factor value of the sample is about 10^6. The enhancement factor value calculated by such method is usually under-evaluated due to the difficulty to determine the exact value of N_{ads},[33] Thus we believe that the real enhancement factor could be in the order of 10^7. As shown in Figure S2, the Ag nanoshell arrays show much larger SERS enhancement than Ag nanoparticle films produced by conventional mirror reaction.

It is worth noting that, unlike the conventional methods for preparing SERS substrates that often need chemical additives and thus produce by-products on the substrate surface, the method involving the laser ablation and the electrophoresis presented in this work is a clean fabrication process without additives and by-products. The obtained Ag nanoshells have a ''naked'' and clean highly roughened surface, which is undoubtedly beneficial to SERS performances.

2.5. General Applicability of the Fabrication Strategy

The fabrication process presented in this article, which can realize large-scale Ag nanoshell arrays with well-defined structures and tunable properties, could be extended to the nanoshell arrays of other materials, such as Au, Pt, and TiO_2. Moreover, hybrid multiple-layered nanoshell arrays could also be fabricated by multi-step electrophoresis in different colloidal solutions (such as Ag/Au and Pt/TiO_2), which is in progress.

3. Conclusions

In summary, this work presents an important surface nanopatterning technique for fabricating large-scale ordered arrays of nanoshells with well-defined structures. Using an electrophoresis of Ag colloidal solutions on PS sphere templates, regular arrayed Ag nanoshells are prepared with high structural controllability. Based on the adjustment of the structural parameters including the diameter, the surface roughness, and the intershell spacing of nanoshells, properties of the nanoshell arrays, such as the SERS and LSPR properties, can be controlled. The well-defined surface patterns of Ag nanoshells could be used as the candidate structures for SERS sensors, lithium-ion batteries, solar cells, and optical devices. Moreover, the surface nanopatterning technique presented in this study has universality and could be extended to the nanoshell arrays of the other materials including metals, semiconductors, and metallic oxides.

4. Experimental

Preparation of Ag Colloidal Solutions: The Ag colloidal solution was prepared by laser ablation of an Ag flake (purity higher than 99.9%) immersed in deionized water. First, the Ag flake was ultrasonically cleaned in deionized water for 1 h and ethanol for 1 h, respectively. Then the Ag flake was immersed in deionized water (8 mL in a vessel). The flake was irradiated by the first harmonic (1064 nm) Nd:YAG laser operating at 150 mJ per pulse with a pulse duration of 10 ns and a frequency of 10 Hz. The laser beam was focused with a spot size of about 2 mm in diameter on the flake, using a lens with a focal length of 150 mm. The solution was continuously stirred during the irradiation process. After 30 min irradiation, a yellowish Ag colloidal solution was obtained.

Preparations of PS Sphere Templates: The monolayer PS sphere arrays with an area of about 1 cm^2 were prepared by a spin-coating process [34–36]. First, glass slides were washed in turn with ethanol, H_2SO_4:H_2O_2 (3:1), H_2O:$NH_3 \cdot H_2O$:H_2O_2 (5:1:1), and deionized water. Suspensions of monodisperse PS spheres (with three different diameters of 750 nm, 1 μm, and 2 μm; 2.5 wt% in water; surfactant free) were obtained from Alfa Aesar Corporation. After ultrasonic vibration, 10 μL of the PS suspension was pipetted onto a glass slide mounted on a spin-coater. The close-packed monolayer PS sphere templates were formed by the spin-coating process, and the PS sphere monolayer was then floated onto the surface of deionized water. After that, the PS sphere monolayer was picked up on a new substrate (Si or ITO), followed by heating at 110 °C for 10 min to enhance the adhesion of PS sphere layer on the substrate (the cleaning process of Si or ITO substrates for the growth of PS sphere monolayer is much more complicated than that of glass slides, that's the reason why we first prepared the PS sphere monolayer on glass slides and then transfer it to Si or ITO substrates). Non-close-packed PS sphere arrays were prepared by a plasma etching process on the close-packed PS sphere arrays. The close-packed PS spheres were exposed to argon plasma reactor (PDC-32G-2) at 70 Pa. Radio frequency with a 100 W power was applied after an equilibrium pressure was reached. The spacing between neighboring PS spheres can be controlled by the plasma etching time. Such templates have been widely used to prepare metallic triangular nanoparticle arrays through thermal evaporation methods [37,38]. Here, we develop a new application of these templates to fabricate well-defined nanoshell arrays.

Electrophoretic Deposition Process: First, a thin Ag film with a thickness of about 3 nm was deposited on the PS sphere template using a lab-made sputtering system. Then the PS sphere arrays, covered with the thin Ag film, were immersed into the Ag colloidal solution and used as the cathode. The electrophoretic deposition was performed under a constant deposition current density. Different current densities (10, 50, and 100 μA cm^{-2}) were used to control the mean size of the Ag nanoparticles in nanoshells.

Characterizations: The morphology of Ag nanoshells was observed by a SEM (FE-SEM, Sirion 200 FEG). TEM measurement was conducted on a JEM-200CX TEM operated at 200 kV. The extinction spectra were measured on a Cary-5E UV-Vis-NIR spectrophotometer. 10 μL R6G aqueous solution (10^{-6} mol L^{-1}) was dropped on the sample surface before Raman spectral examination. The Raman scattering spectra were recorded using a confocal microprobe Raman system (LABRAM-HR). All the samples were examined for 5 times at different positions. The deviation is within 10%. The excitation wavelength was 532 nm with a fluence of 0.2 mW cm^{-2}. The accumulation time was maintained at 5 s.

Acknowledgements

This work is a collaborative work between the Chinese Academy of Sciences and the University of Muenster. It was financially supported by the Natural Science Foundation of China (50831005), the Major State research program of China (2006CB300402), the European Research Council Starting Grant (ThreeDSurface), the Volkswagen Foundation, and German Research Foundation (DFG, TRR61). Supporting Information is available online from Wiley InterScience or from the author.

Received: March 11, 2010
Revised: April 14, 2010
Published online: June 28, 2010

[1] W. Wang, Z. Li, B. Gu, Z. Zhang, H. Xu, *ACS Nano.* **2009**, *3*, 3493.
[2] K. N. Heck, B. G. Janesko, G. E. Scuseria, N. J. Halas, M. S. Wong, *J. Am. Chem. Soc.* **2008**, *130*, 16592.
[3] Y. Wang, F. Su, J. Lee, X. S. Zhao, *Chem. Mater.* **2006**, *18*, 1347.
[4] H. Kim, B. Han, J. Choo, J. Cho, *Angew. Chem. Int. Ed.* **2008**, *47*, 1.
[5] R. Teki, M. K. Datta, R. Krishnan, T. C. Parker, T. Lu, P. N. Kumta, N. Koratkar, *Small.* **2009**, *5*, 2236.
[6] J. Qian, P. Liu, Y. Xiao, Y. Jiang, Y. Cao, X. Ai, H. Yang, *Adv. Mater.* **2009**, *21*, 3663.
[7] S. A. Maier, M. L. Brongersma, P. G. Kik, S. Meltzer, A. G. Requicha, H. A. Atwater, *Adv. Mater.* **2001**, *13*, 1501.
[8] Y. D. Yin, R. M. Rioux, C. K. Erdonmez, S. Hughes, G. A. Somorjai, A. P. Alivisatos, *Science.* **2004**, *304*, 711.
[9] J. H. Yang, T. Sasaki, *Chem. Mater.* **2008**, *20*, 2049.
[10] G. Decher, *Science.* **1997**, *277*, 1232.
[11] D. Li, J. Zhang, K. Landskron, T. Liu, *J. Am. Chem. Soc.* **2008**, *130*, 4226.
[12] Y. Sun, Y. Xia, *Science.* **2002**, *298*, 2176.
[13] J. Y. Chen, J. M. Mclellan, A. Siekkinen, Y. J. Xiong, Z. Y. Li, Y. N. Xia, *J. Am. Chem. Soc.* **2006**, *128*, 14776.
[14] X. Lu, H. Tuan, J. Chen, Z. Li, B. A. Korgel, Y. N. Xia, *J. Am. Chem. Soc.* **2007**, *129*, 1733.
[15] J. B. Lassiter, M. W. Knight, N. A. Mirin, N. J. Halas, *Nano Lett.* **2009**, *9*, 4326.
[16] C. H. Kuo, T. Hua, M. H. Huang, *J. Am. Chem. Soc.* **2009**, *131*, 17871.
[17] X. L. Xu, S. A. Asher, *J. Am. Chem. Soc.* **2004**, *126*, 7940.
[18] For example, the calculated number of all the crevices in a 750 nm sized nanoshell covered by 60 nm sized nanoparticles is 2200. Here we hypothesize the surface of the PS sphere is covered by uniform 60 nm sized Ag nanoparticles and there is only one crevice between two adjacent particles, thus the number of the Ag nanoparticles and the crevices on the nanoshell can be calculated.
[19] S. K. Yang, W. P. Cai, G. Q. Liu, H. B. Zeng, *J. Phys. Chem. C* **2009**, *113*, 7692.
[20] Regarding the fact that the thickness of Ag nanoshells is much smaller than the diameters of PS spheres, the diameter of nanoshells mainly depends on the diameter of PS spheres.
[21] C. F. Bohren, D. R. Huffman, *Absorption and Scattering of Light by Small Particles*, Wiley, New York **1998**.
[22] E. Prodan, C. Radloff, N. J. Halas, P. Nordlander, *Science.* **2003**, *302*, 419.
[23] J. B. Lassiter, J. Aizpurua, L. I. Hernandez, D. W. Brandl, I. Romero, S. Lal, J. H. Hafner, P. Nordlander, N. J. Halas, *Nano Lett.* **2008**, *8*, 1212.
[24] E. Prodan, P. Nordlander, *Nano Lett.* **2003**, *3*, 543.
[25] E. Prodan, P. Nordlander, N. J. Halas, *Nano Lett.* **2003**, *3*, 1411.
[26] Y. Sun, Y. Xia, *Anal. Chem.* **2002**, *74*, 5297.
[27] S. Lal, N. K. Grady, J. Kundu, C. S. Levin, J. B. Lassiter, N. J. Halas, *Chem. Soc. Rev.* **2008**, *37*, 898.
[28] K. Kneipp, Y. Wang, H. Knipp, T. Perelman, I. Itzkan, R. R. Dasari, M. S. Feld, *Phys. Rev. Lett.* **1997**, *78*, 1667.
[29] A. M. Michaels, M. Nirmal, L. E. Brus, *J. Am. Chem. Soc.* **1999**, *121*, 9932.
[30] S. J. Lee, A. R. Morrill, M. Moskovits, *J. Am. Chem. Soc.* **2006**, *128*, 2200.
[31] S. M. Nie, S. R. Emory, *Science.* **1997**, *275*, 1102.
[32] S. R. Emory, W. E. Haskins, S. M. Nie, *J. Am. Chem. Soc.* **1998**, *120*, 8009.
[33] G. Q. Liu, W. P. Cai, L. C. Kong, G. T. Duan, F. J. Lü, *J. Mater. Chem.* **2010**, *20*, 767.
[34] F. Q. Sun, W. P. Cai, Y. Li, B. Q. Cao, Y. Lei, L. D. Zhang, *Adv. Funct. Mater.* **2004**, *14*, 283.
[35] Y. Li, W. P. Cai, G. T. Duan, *Chem. Mater.* **2008**, *20*, 615.
[36] Y. Li, T. Sasaki, Y. Shimizu, N. Koshizaki, *J. Am. Chem. Soc.* **2008**, *130*, 14755.
[37] C. L. Haynes, R. P. Van Duyne, *Nano Lett.* **2003**, *3*, 939.
[38] A. V. Whitney, B. D. Myers, R. P. Van Duyne, *Nano Lett.* **2004**, *4*, 1507.